The most extreme rainfall erosivity event ever recorded in China: The "7.20" ~~rain~~storm in Henan ~~Province~~province

Yuanyuan Xiao[1], Shuiqing Yin[1], Bofu Yu[2], Conghui Fan[1], Wenting Wang[1], Yun Xie[1]

[1]State Key Laboratory of Earth Surface Processes and Resource Ecology, Faculty of Geographical Science, Beijing Normal University, Beijing, 100875, China
[2]Australian Rivers Institute, School of Engineering and Built Environment, Griffith University, Nathan, Queensland, QLD 4111, Australia

Correspondence to: Shuiqing Yin (yinshuiqing@bnu.edu.cn)

Abstract. Severe water erosion occurs during extreme storm events. Such an exceedingly severe~~extreme~~ storm occurred in Zhengzhou in central China on 20 July 2021 (the "7.20" ~~rain~~storm). The magnitude and frequency of occurrence of this storm event were examined in terms of how erosive it was~~its erosivity values~~. To contextualize this extreme event, hourly rainfall data from 2420 automatic meteorological stations in China from 1951 to 2021 were analyzed to: (1) characterize the spatial and temporal distribution of rainfall amount and rainfall erosivity of the "7.20" ~~rain~~storm, (2) evaluate the average recurrence interval of the maximum daily and event rainfall erosivity, and (3) establish the geographical distribution of the maximum daily and event rainfall erosivity in China. The center of the "7.20" ~~rain~~storm moved from southeast to northwest in Henan province, and the most intense period of rainfall occurred in the middle and late stages of the storm. Zhengzhou meteorological station happened to be aligned with the center of the storm, with a maximum daily rainfall of 552.5 mm and a maximum hourly rainfall intensity of 201.9 $mm \cdot h^{-1}$. The average recurrence intervals of the maximum daily rainfall erosivity (43,354 $MJ \cdot mm \cdot ha^{-1} \cdot h^{-1}$) and the maximum event rainfall erosivity (58,874 $MJ \cdot mm \cdot ha^{-1} \cdot h^{-1}$) ~~was~~ were estimated to be about ~~109,079~~10,000 and 23,100~~154,154~~ years, respectively, assuming the log Pearson type III ~~generalized extreme value~~ distribution, and these were the maximum rainfall erosivity ever recorded among 2420 meteorological stations in mainland China. The "7.20" ~~rain~~storm suggests that the most erosive of storms does not necessarily occur in the wettest places in southern China, and it can occur in mid-latitude around 35 °N with a moderate mean annual ~~precipitation~~ rainfall of ~~549.2~~566.7 mm in Zhengzhou ~~meteorological station~~.

Keywords. soil erosion, extreme rainfall, rainfall erosivity, the return period

带格式的: 字体: 非加粗

1 Introduction

Soil erosion ~~is known~~ as a land degradation process that can affect food production, biodiversity, carbon stocks and ecosystem services (Kebede et al. 2021; Panagos et al., 2015). Soil erosion models are powerful tools to evaluate the rate of erosion ~~intensity~~ and the effect of soil and water conservation measures for decision makers. The Universal Soil Loss Equation (USLE) (Wischmeier and Smith, 1965, 1978) and the~~its~~ revised USLE (Renard et al., 1997; USDA–ARS, 2013), and the Chinese Soil Loss Equation (CSLE, Liu et al., 2002) are widely used empirical soil erosion prediction models for estimating the long-term average amount of soil loss. Rainfall erosivity quantifies the potential ability of rainfall and runoff to erode the soil and represents the climatic effect on soil erosion as one of the factors in the USLE, RUSLE and CSLE (Yin et al., 2017).

~~Research has focused on the calculation and estimation of rainfall erosivity, and its spatial and temporal variations (Yin et al., 2017). High temporal resolution data are often used to estimate the rainfall erosivity ranging between 1-min and 60-min intervals in most studies (Klik et al., 2015; Lu and Yu, 2002; Ma et al., 2014; Panagos et al., 2015, 2016; Xie et al., 2016; Yin et al., 2015;). As rainfall data with high temporal resolution in most parts of the world are limited in terms of the record length and spatial coverage, it is often necessary to establish simple relationships between rainfall erosivity values based on data with~~

~~finer and coarser resolutions, and then apply these relationships to regions with data in coarser resolution only (Xie et al., 2016; Yin et al., 2015; Zhu and Yu, 2015). Since soil erosion is difficult to measure at large scales, soil erosion models are often used for estimating soil loss by water erosion at regional, national and global scales. Rainfall erosivity maps can provide rainfall erosivity values with rainfall observations and without observations and the generation of erosivity maps is one of necessary procedures for estimation of soil loss using most empirical soil erosion models (Bezak et al. 2021, 2022; McGehee et al., 2022; Yue et al., 2022). Rainfall erosivity maps were usually generated by the interpolation of rainfall erosivity values from at-site rainfall observations by geostatistics techniques, such as the inverse distance weighting, ordinal Kriging and so on (Panagos et al., 2015; Sadeghi et al., 2017; Yin et al., 2019). Available gridded rainfall data, such as satellite precipitation products and climate reanalysis data can also be used to generate rainfall erosivity maps (Panagos et al., 2017; McGehee et al., 2022; Yue et al., 2022). Auerswald et al. (2019) used 1 km resolution radar rainfall data to produce the average rainfall erosivity maps with 1 km in resolution in Germany from 2001 to 2017. Temporal variations in rainfall erosivity are important for understanding changes in soil erosion and assessing the future climate change impact on the land degradation. At present, research on the temporal change of rainfall erosivity mainly focuses on past changes (Cao et al., 2018; Qin et al.2016; Wang et al., 2022; Yang, 2015; Zhang et al, 2010) and future projections (Kilic et al 2021; Panagos et al., 2022).~~

Most studies have focused on the long-term average of rainfall and rainfall erosivity characteristics (Gu et al., 2020; Li et al., 2008; Liu et al. ~~2019~~2018; Yin et al., 2019), and have assessed the intensity and frequency of extreme rainfall events at the regional, national and global ~~levels~~ scales (Alexander et al., 2007; Almagro et al., 2017; Evans et al., 2016; Nearing et al., 2004). However, there ~~are~~ have been few studies of rainfall erosivity ~~of~~ during extreme events (Diodato et al., 2016; Wang et al., 2022). The long-term average value cannot fully ~~reflect~~ represent the severity of the soil erosion process, and a few severe soil erosion events can contribute a great deal to the total amount of soil lost over many years (Bezak et al. 2021; Borrelli et al., 2016; Meusburger et al., 2012; Petek et al., 2018). For example, field observations at the plot scale in eastern Austria showed that the three largest erosion events from 1994 to 2019 accounted for 79% of the total soil loss over the same period (Klik and Rosner, 2020). Zhou et al. (1992) reported that high-intensity, short-duration heavy precipitation events accounted for about 90% of the total annual soil erosion in the Loess Plateau region.

Extreme rainfall, which varies a great deal in space and time, can lead to severe flooding, with far-reaching implications for socio-economic and human activities (Fishman, 2016). With global warming, the frequency and intensity of extreme precipitation events are increasing ~~in most~~mostly in mid-latitudes (Fang et al., 2017; IPCC 2021; Liao et al., 2019; Liu et al., 2017). Extreme rainfall, especially rainfall events with high intensity, is often more erosive (Fang et al., 2018; Huang et al., 2016a, 2016b, 2016c). Many studies reported that satellite-based products tended to underestimate the extreme rainfall, which can have an important effect on the estimation of rainfall erosivity ~~based on~~using satellite-based products (Jiang et al., 2019; Palharini et al., 2020; Rahmawati and Lubczynski., 2018). For example, Bezak et al. (2022) showed CMORPH estimates had a marked tendency to underestimate rainfall erosivity ~~of~~ in highly erosive areas when compared to the the GloREDa estimates. In addition, underestimation of extreme rainfall from climate models will ~~cause~~ lead to conservative projections of erosivity in highly erosive areas in the future (Panagos et al., 2022). Therefore, it is of great interest to examine the magnitude and frequency of occurrence of rainfall and rainfall erosivity of extreme storm events.

An extraordinarily heavy rainfall event occurred between 17th and 22th of July 2021 in Henan ~~Province~~province. Such a rare event was never experienced or recorded in recent times in China. Record daily rainfall was observed at 10 ~~national~~ meteorological ~~observation~~ stations in Zhengzhou, Xinxiang, Kaifeng, Zhoukou, Luoyang and other cities in Henan ~~Province~~province. Zhang et al. (2021) reported that the storm was influenced by several weather systems including the eastward extension of the South Asian high, the abnormal northerly subtropical high, the Bengal Bay Depression at low latitude, the typhoon "Chapaca"~~Cempaka~~ in the South China Sea and the typhoon "Fireworks" in the Western Pacific. The strengthened and eastward extension of the South Asia high leads to an obvious divergence area of the upper atmosphere over Henan

带格式的：上标

带格式的：上标

~~Province~~province, which is conducive to the upward movement of the lower atmosphere. The subtropical high, which is ~~stronger and~~ northward moving and stronger than ~~the same period in normal years~~usual for the same period, the No. 6 typhoon "Fireworks" and the No. 7 typhoon "Chapaca" in low latitudes, and the low pressure in Bengal Bay have led to the stable and lasting transmission of warm and humid air-flow to Henan ~~Province~~province (Zhang et al., 2021; Qian et al., 2022).~~.~~ Taihang Mountains and Funiu Mountains in the northwestern and western Henan ~~Province~~ province blocked the air-flow, and a strong convergence formed in front of mountains, resulting in this extreme rainfall event.

The maximum hourly rainfall between 16:00 and 17:00 on 20 July reached 201.9 mm at Zhengzhou meteorological station, the highest ever recorded in China (Zhang et al., 2021). It has been widely reported that this extreme storm caused extensive flooding and landslides with damages to infrastructure and loss of human lives (Jin et al., 2022; Zhang et al., 2022). Event total rainfall, daily and hourly rainfall of the "7.20" ~~rain~~storm have been reported elsewhere (Zhang et al. 2021), whereas rainfall erosivity associated with this extreme storm has not~~but rainfall erosivity associated with this extreme storm is still unknown.~~ The "7.20" ~~rain~~storm presents a rare opportunity to examine the extreme rainfall erosivity in China. ~~Thus~~For this study, hourly rainfall data were used to evaluate the maximum daily and event rainfall erosivity, to estimate its average recurrence interval, to contextualize geographically the extreme erosivity of the "7.20" ~~rain~~storm, to demonstrate how extreme the erosivity value of the "7.20" ~~rain~~storm was and how large event rainfall erosivity could be in China, and to highlight the need to pay attention to extreme storm events ~~s~~ and the huge erosion risk associated with them in the future.

2 Material and Methods

2.1 Data source and pre-processing

Observed hourly rainfall data from 1951 to 2021 for 2420 meteorological stations in China were collected by siphon rain gauges or tipping bucket rain gauges. The rainfall data acquired from China Meteorological Administration (CMA) and the data had been quality-controlled by CMA's National Meteorological Information Center. However, we found some unexpected errors in the data, so we checked hourly with daily observation from rain gauges. Hourly observations in early days were mainly digitized from precipitation autographic charts on paper. From 2000 to 2005, automatic weather stations were put into use and their introduction was gradually accelerated. Since 2005, nearly all observations were recorded with automatic weather stations. Hourly rainfall data from ~~797~~ 796 meteorological stations in Henan and its surrounding nine provinces (municipalities) from 20:00 (Beijing time) on 16 July and to 20:00 on 22 July 2021 were used to characterize the "7.20" ~~rain~~storm. Hourly rainfall data from 1951 to 2020 were used to calculate the annual maximum daily and event rainfall erosivity.~~as historical data. In order to~~To reduce the impact of missing values on the result, years with missing data were discarded. A year with missing data was defined as follows: if there were ~~4~~ four or more hours of missing records on a given day, it was considered as a missing day and if the number of missing days in a month ≥ ~~6~~six, it was considered as a missing month. Since most of the rainfall in the north of China (north of 32°N) is concentrated from May to September, the year with any month from May to September missing was defined as a missing year. In ~~the south of~~southern China (south of 32°N), the year with any month from April to October missing is defined as a missing year. Missing years were removed, and ~~Missing~~ missing values in effective years are input as ~~0~~zero value.

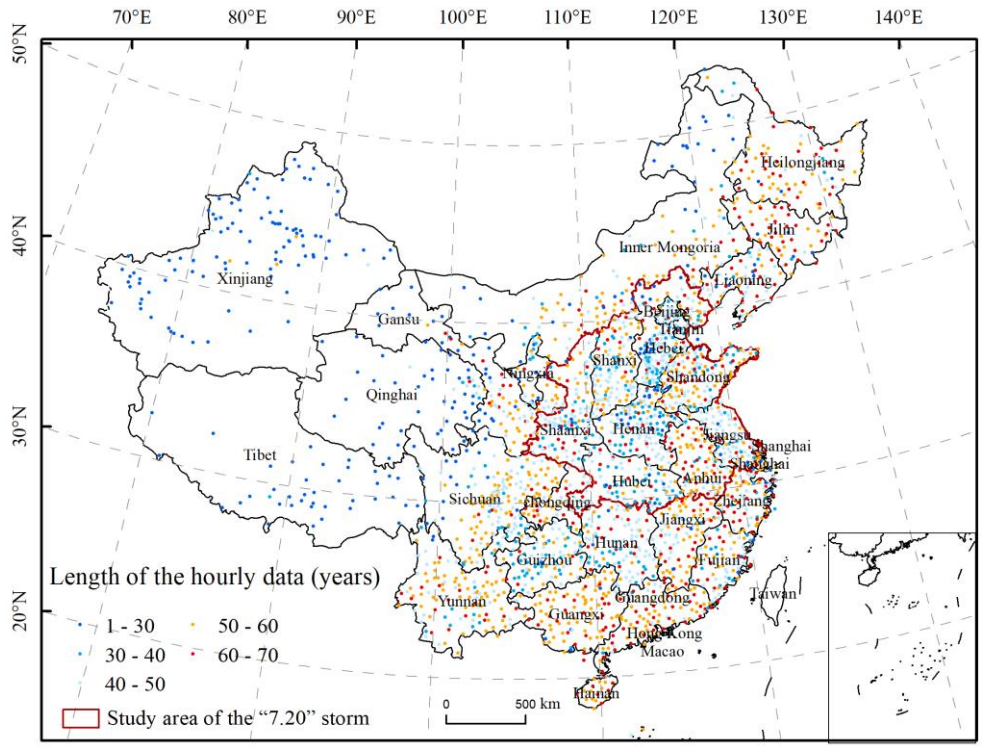

Figure 1. Spatial distribution of stations with hourly rainfall data and the record length.

2.2 Framework of study

2.2.1 Definition of rainfall events and rainfall parameters

An event was defined as ~~the duration~~a period of rainfall separated with dry periods ~~less~~ greater than "minimum inter-event time" (MIT). The MIT in the USLE and RUSLE2 was ~~6~~ six hours. In this study, MIT of six hours was used to define rainfall events.~~the storm was divided into events when the time of no rainfall was over 6 hours.~~ The maximum event rainfall, maximum daily rainfall, maximum hourly rainfall and maximum event rainfall erosivity were computed following to the framework ~~of~~ shown in Fig. 2. Since ~~There~~ there were ~~several erosive~~multiple events over the ~~6~~six-day in period during the "7.20" ~~rain~~storm~~.~~ ~~T~~, the maximum event rainfall was the maximum rainfall amount of all events over the six-days period.~~associated with the erosive event with the maximum rainfall amount, and it was not the total rainfall amount over the 6 days.~~ Maximum event rainfall erosivity was similarly defined.

2.2.2 Calculation of the energy and daily/event rainfall erosivity

~~Erosive events~~Hourly data were used to calculate the ~~daily and event~~ rainfall erosivity, EI_{30} (MJ·mm·ha^{-1}·h^{-1})for each event, which is the product of the event energy and peak 30-min intensity. All the hourly data for day (8:00 pm to 8:00 pm) were used to compute daily rainfall erosivity.

Rainfall kinetic energy is used by most erosion models for assessing the capacity of rainfall to produce erosion. Rainfall kinetic energy is a function of raindrop size and falling velocity. Because the direct measurement of kinetic energy (KE) requires

complex and expensive instruments, many different estimation methods have been developed. These methods use logarithmic, exponential, or power law formulas to derive kinetic energy-intensity (KE-I) relationships. The most widely accepted kinetic energy-intensity relationship is the exponential model proposed by Kinnell (1981). The rainfall kinetic energy is calculated by Eq. (2), which includes the modification suggested by McGregor et al. (1995).

~~Rainfall kinetic energy is a function of raindrop size and falling velocity.~~ The total energy (EN, MJ·ha^{-1}) of an erosive event was ~~estimated~~ computed using ~~the~~ following equations (USDA-ARS, 2013):

~~$e_r = 0.29 \cdot [1 - 0.72 \cdot exp(-0.082 \cdot i_r)]$~~ ~~(1)~~

$$EN = \sum_{r=1}^{l}(e_r \cdot P_r) \quad (1)$$

$$e_r = 0.29 \cdot [1 - 0.72 \cdot exp(-0.082 \cdot i_r)] \quad (2)$$

where a rainfall event was divided into l periods, each with a ~~constant~~n intensity, i_r (mm·h^{-1}) ~~, for the r^{th} period,~~ P_r (mm) was the rainfall amount for the r^{th} period and e_r (MJ·mm^{-1}·ha^{-1} ~~·mm^{-1}~~) was the ~~unit~~ energy per unit rainfall per unit area ~~(MJ·mm^{-1}·ha^{-1})~~ for the r^{th} period. The event rainfall erosivity can be estimated with of EN and I_{1h} (USDA-ARS, 2013):

$$EI_{1h} = EN \cdot I_{1h} \quad (3)$$

$$EI_{30} = 1.489 \cdot EI_{1h} \quad (4)$$

where I_{1h} was the peak ~~1~~one-hour rainfall intensity for the erosive event, and the conversion factor of 1.489 was used to correct the bias ~~of estimated~~in the rainfall erosivity using hourly rainfall data (Yue et al., 2020).

Total rainfall and energy over the six~~6~~ days of the "7.20" ~~rain~~storm for 796 stations were interpolated into grid data with 100 m spatial resolution, and regional averages of Henan province and the study area (Henan province and its surrounding nine provinces/municipalities) were calculated and compared with Zhengzhou meteorological station. We used inverse distance weighting (IDW) to interpolate point data to map rainfall erosivity distribution for the region.

2.2.3 *Log Pearson type III distribution* ~~*Generalized extreme value distribution model and parameter estimation*~~

An annual series is defined here as a collection of maxima, one from each calendar year. Annual series of the maximum daily and event rainfall erosivity from the period 1951-2020 (n = 67 due to three missing years) for Zhengzhou meteorological station were sorted in a descending order with the largest assigned a rank of ~~1~~one. The empirical return period, or the average recurrence interval, of each observation in the annual series was calculated according to the following formula (Bobeé and Robitaille, 1977):

$$RP = \frac{n+1}{m} \quad (5)$$

where RP is the empirical return period in years, n was the number of years or the sample size, and m *was* the rank (m = 1 for the largest).

The probability distribution used to fit the annual series was the log Pearson type III (LP-Ⅲ) distribution. LP-Ⅲ distribution is considered a suitable model for flood frequency estimation in many investigations (Bobeé and Robitaille, 1977; England et al., 2003; England, 2019). The logarithms of the annual series of the maximum daily rainfall erosivity and the maximum event rainfall erosivity from 1951-2020 for Zhengzhou meteorological station were used to fit the Pearson type III distribution (P-III), respectively. ~~The annual series of the maximum daily rainfall erosivity and the annual maximum event rainfall erosivity from 1951-2020 for Zhengzhou meteorological station were used to fit the Generalized Extreme Value (GEV) distribution, respectively. The probability distribution function of GEV can be expressed (Li et al., 1988; Huang et al., 2020) as:~~

~~$F(x) = e^{-(1+k\frac{x-\mu}{\sigma})^{-\frac{1}{k}}}$~~ ~~(6)~~

$$f(x) = \frac{\beta^{\alpha}}{\Gamma(\alpha)}(x-a_0)^{\alpha-1}e^{-\beta(x-a_0)} \quad x > a_0, \alpha > 0, \beta > 0 \quad (6)$$

$$F(x) = \frac{\beta^{\alpha}}{\Gamma(\alpha)}\int_{a_0}^{x}(x-a_0)^{\alpha-1}e^{-\beta(x-a_0)}dx \quad (7)$$

带格式的: 缩进: 首行缩进: 0 厘米

带格式的: 字体: (中文) +中文正文 (等线)

带格式的: 两端对齐, 缩进: 首行缩进: 0 厘米, 制表位: 47.49 字符, 右对齐

where x is the random variable of interest, a_0 was the location parameter, α the shape parameter, and β the scale parameter. $\Gamma(\alpha)$ is the gamma function. The basic parameters, mean $\bar{x}$, coefficient of variation C_V, and skewness coefficient C_S, were used to estimate parameter a_0, α and β (Viessman Jr. and Lewis, 2002) (Eq. 8-10), and the 95% confidence interval was also estimated (Kite, 1975). ~~where k was the shape parameter, σ the scale parameter and μ the position parameter. The estimated value of rainfall erosivity with a return period T is X_T as follows:~~

$$\alpha = \frac{4}{C_s^2} \quad (8)$$

$$\beta = \frac{2}{\bar{x}C_sC_v} \quad (9)$$

$$a_0 = \bar{x}\left(1 - \frac{2C_v}{C_s}\right) \quad (10)$$

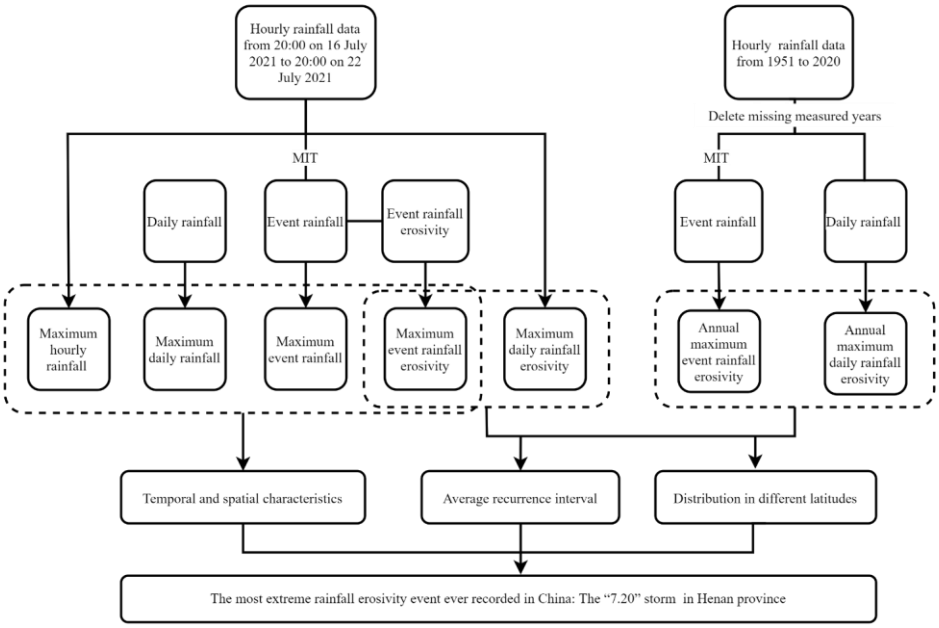

~~$$X_T = \begin{cases} \mu + \frac{\sigma}{k}\left\{1 - \left[-log\left(1 - \frac{1}{T}\right)\right]^{-k}\right\} & k \neq 0 \\ \mu + \sigma\left\{1 - \left[-log\left(1 - \frac{1}{T}\right)\right]\right\} & k = 0 \end{cases} \quad (7)$$~~

~~where log is natural log. Method of L-moments was used for the parameter estimation (Hosking, 1990). L-moments is a linear combination of probability weighted moments (PWMs), and the estimated value has good robustness. Among them, the r^{th} order probability weighted moment of random variable x is:~~

~~$$B_r = E[x \cdot F(x)^r] \quad (8)$$~~

~~By sorting sample of size n from the smallest to the largest, the following estimates can be obtained:~~

~~$$\widehat{b_0} = \frac{1}{n}\sum_{j=1}^{n} x_j \quad (9)$$~~

~~$$\widehat{b_1} = \frac{1}{n}\sum_{j=1}^{n-1} \frac{(n-j)}{(n-1)} x_j \quad (10)$$~~

~~$$\widehat{b_2} = \frac{1}{n}\sum_{j=1}^{n-2} \frac{(n-j)(n-j-1)}{(n-1)(n-2)} x_j \quad (11)$$~~

$$\widehat{b_3} = \frac{1}{n}\sum_{j=1}^{n-3}\frac{(n-j)(n-j-1)(n-j-2)}{(n-1)(n-2)(n-3)}x_j \quad (12)$$

L-moments can be obtained by a linear combination of the above estimates:

$$l_1 = \widehat{b_0} \quad (13)$$

$$l_2 = 2\cdot\widehat{b_1} - \widehat{b_0} \quad (14)$$

$$l_3 = 6\cdot\widehat{b_2} - 6\cdot\widehat{b_1} + \widehat{b_0} \quad (15)$$

$$l_4 = 20\cdot\widehat{b_3} - 30\cdot\widehat{b_2} + 12\cdot\widehat{b_1} - \widehat{b_0} \quad (16)$$

where τ_3 is l-skewness, τ_4 is l-kurtosis, which can be calculated with the ratio of L-moments:

$$\tau_3 = \frac{l_3}{l_2},\ \tau_4 = \frac{l_4}{l_2} \quad (17)$$

From the set of equations above, parameters of the GEV distribution can be estimated:

$$\hat{z} = \frac{2}{3+\tau_3} - \frac{ln2}{ln3} \quad (18)$$

$$\hat{k} \approx 7.859\cdot\hat{z} + 2.9554\cdot\hat{z}^2 \quad (19)$$

$$\hat{\sigma} = \frac{l_2\cdot\hat{k}}{(1-2^{-\hat{k}})\cdot\Gamma(1+\hat{k})} \quad (20)$$

$$\hat{\mu} = l_1 + \hat{\sigma}\frac{\Gamma(1+\hat{k})-1}{\hat{k}} \quad (21)$$

where $\Gamma(\cdot)$ is the gamma function.

Figure 2. Study Framework for this study

3 Results and discussion

3.1 Temporal and spatial characteristics of the "7.20" rainstorm

3.1.1 Characteristics of the "7.20" rainstorm

The extreme event occurred in Henan Province province between 20:00 on 16 July 2021 and 20:00 on 22 July 2021. The center of the storm center is mainly located around Zhengzhou. The storm duration was long and accumulated rainfall was huge. Spatial pattern of accumulated rainfall from 20:00 on 16 July 2021 to 20:00 on 22 July 2021of the "7.20" storm is shown in Fig. 3a. The top three rainfall stations were Zhengzhou (817.3 mm), Huixian (755.2 mm) and Xinmi (723.5 mm). Additionally, among the 797 automatic meteorological stations in the study area, 58 meteorological stations have accumulated rainfall of more than 250 mm, of which 50 are located in Henan Provinceprovince. Rainfall mass curves for these three stations are shown in Fig. 3b. Obviously, the rainstorm at Zhengzhou meteorological station and Xinmi station contributed more than 50 % of the rainfall in the middle period, while the rainstorm at Huixian station contributed more than 50 % of the rainfall in the last period. Wang et al. (2016) has have demonstrated that different rainstorm patterns with rainfall peak in the early, middle and late stages have different effects on soil erosion process, under the natural rainfall conditions. n that study, storms were classified into four patterns: the advanced, intermediate, delayed, and uniform depending when rainfall is most concentrated. The dimensionless durations were separated into three equal periods. Advanced pattern, intermediate pattern and delayed pattern when more than 40 % of the rainfall occurs in the first, second and third periods, respectively. The rainfall temporal distribution is regarded as the uniform pattern otherwise. Wang's research showed that given the same EI30, the rainstorm pattern with rainfall peak at the later stage produced more soil loss than the other patterns (Wang et al., 2016). It showed that given the same EI_{30}, the rainstorm pattern with rainfall peak at the later stage produced more soil loss than the other patterns.

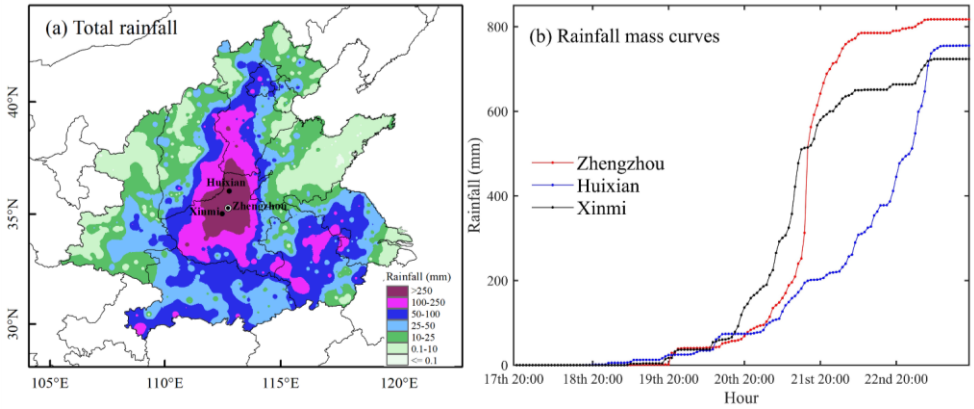

Figure 3. Distribution of total rainfall over the study area~~, Total rainfall over the study area from 20:00 on 16 July 2021 to 20:00 on 22 July 2021,~~ and rainfall mass curves for ~~3~~ three stations with the largest rainfall totals.

Spatial pattern of daily rainfall ~~in study area from 20:00 on 16 July 2021 to 20:00 on 22 July 2021~~of the "7.20" storm in the study area is shown in Fig. 4. Heavy rainfall mainly occured in the middle and late stages of the event. The maximum daily rainfall (Zhengzhou, 552.5 mm) occurred on 20 July (Fig. 4d), while the storm was most extensive on 21 July (Fig. 4e). The storm is initially concentrated in the ~~southeast of Henan and~~ Anhui ~~P~~provinces (Fig. 4a), and then dispersed somewhat on 18 July (Fig. 4b). On 19 July~~-~~, the storm re-appears in the central region of Henan ~~Province~~ province (Fig. 4c). On 20 July, the storm began to intensify and expand its spatial extent (Fig. 4d). The daily rainfall at 39 meteorological stations exceeded 100 mm, and the daily rainfall of ~~7~~ seven meteorological stations exceeded 250 mm on 20 July. On 21 July (Fig. 4e), the center of the storm began to move northward, and the rainfall intensity started to dissipate, and the storm now covered a large area with storm center drifted north to Tangyin (388.2 mm), Henan ~~Province~~province, and recorded rainfall at 48 meteorological stations exceeded 100 mm and ~~6~~ six meteorological stations exceeded 250 mm. The rainfall decreased considerably by 22 July (Fig. 4f). The storm center was located in the north of Henan ~~Province~~province, and the rainfall at 16 meteorological stations exceeded 100 mm.

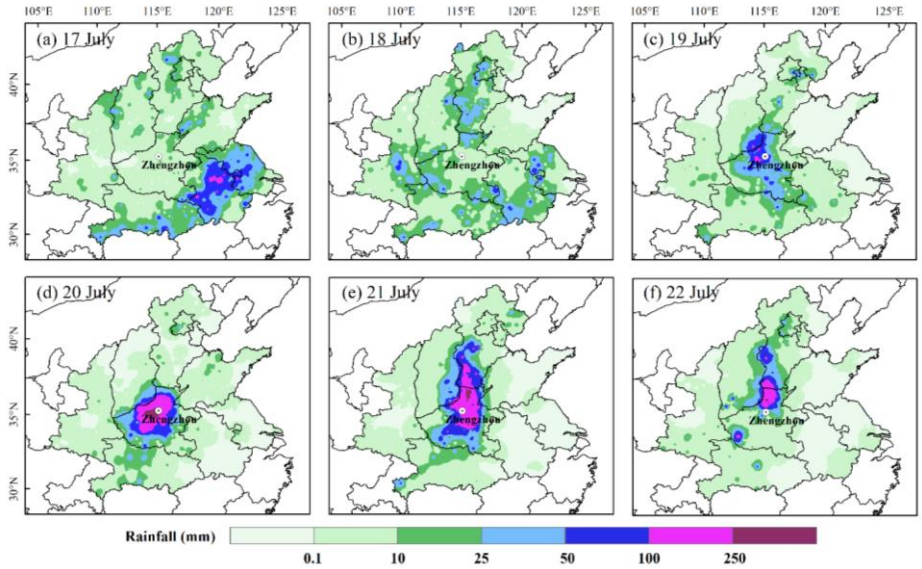

Figure 4. Spatial pattern of daily rainfall in the study area. Daily rainfall is rainfall accumulation over 24-hour period, e.g. daily rainfall on 20 July is the total rainfall from 20:00 on 19 July to 20:00 on 20 July.

3.1.2 The spatial distribution of rainfall parameters and rainfall erosivity

The spatial distribution of maximum daily and hourly rainfall amount, and maximum event rainfall and rainfall erosivity are shown in Fig. 5. At the center of the storm, a maximum event rainfall amount of 785.1 mm and a maximum daily rainfall amount of 552.5 mm on 20 July were recorded at Zhengzhou meteorological station. From 16:00 to 17:00 on 20 July, maximum hourly rainfall reached 201.9 mm at Zhengzhou meteorological station, and created a new hourly rainfall intensity record (201.9 mm·h^{-1}) in mainland China. The maximum event rainfall erosivity in the area with Zhengzhou meteorological station has reached 58,874 MJ·mm·ha^{-1}·h^{-1}.

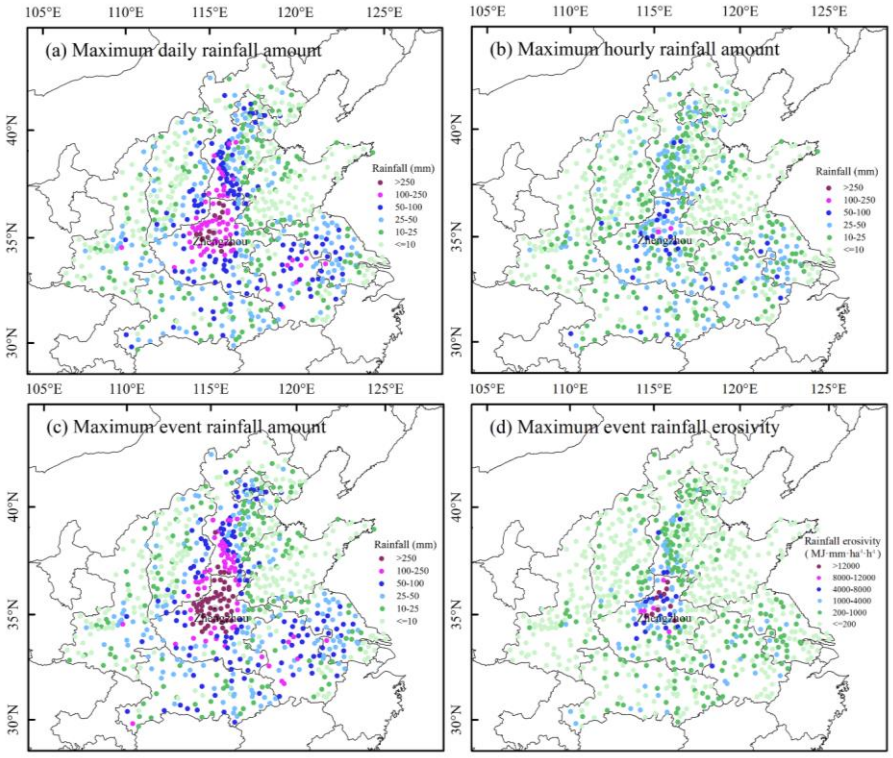

Figure 5. Spatial distribution of rainfall amount and rainfall erosivity associated with the "7.20" ~~rain~~storm.

3.1.3 Rainfall's total kinetic energy

Table 1. The composition of average rainfall and energy in different regions from 20:00 on 16 July 2021 to 20:00 on 22 July 2021

Region	Index	17th	18th	19th	20th	21st	22nd	Total
Study area (1.33×10^8 ha)	Mean rainfall (mm)	12.4	10.0	6.8	8.7	11.3	5.8	55.0
	EN ~~(~~(MJ·ha^{-1})~~)~~	2.6	2.0	1.3	1.7	2.3	1.1	11.0
Henan province (1.66×10^7 ha)	Average rainfall (mm)	5.8	13.5	26.6	70.5	61.9	21.5	199.8
	EN ~~(~~(MJ·ha^{-1})~~)~~	2.0	3.0	4.8	13.5	15.6	7.1	46.0
Zhengzhou meteorological station	Average rainfall (mm)	0.0	1.3	60.2	552.5	176.0	27.3	817.3
	EN（MJ·ha^{-1}~~）~~）	0.0	0.1	12.3	144.2	40.0	4.0	200.6

带格式表格

The detachment of soil particles from the soil mass and the transportation of detached particles by raindrop impact and surface water flow are two main processes of soil erosion. Rainfall energy reflects the impact of raindrop detachment on the soil. The average rainfall and energy for each meteorological day over different regions ~~from 20:00 on 16 July 2021 to 20:00 on 22 July 2021~~of "7.20" storm were listed in Table. 1. Comparing the three regions, the average rainfall and EN in the study area on 17 July are higher than those in Henan ~~Province~~ province and Zhengzhou meteorological station, indicating that the rainstorm center may be outside Henan ~~Province~~ province at this time. With the movement of rainstorm center, the average rainfall and EN of Henan ~~Province~~ province and Zhengzhou meteorological station gradually increase. The average rainfall in Henan p~~P~~rovince reached its peak on 20 July (70.5 mm), but EN reached its peak on 21 July (15.6 MJ·ha^{-1}). The average rainfall and

EN of Zhengzhou meteorological station reached the peak on 20 July, which were 552.5 mm and 144.2 MJ·ha^{-1} respectively. The energy of Zhengzhou meteorological station on 20 July is 11 times of average energy in Henan Pprovince. Land vegetation, including forests, shrubs and grass, provide the important protection from the direct detachment of raindrops.

In summary, an extraordinarily heavy rainfall event occurred in Henan province between 20:00 on 16 July 2021 and 20:00 on 22 July 2021. Among them, the observations of Zhengzhou Meteorological Station show that the maximum event rainfall is 785.1 mm, the maximum daily rainfall is 552.5 mm, the maximum hourly rainfall intensity is 201.9 mm·h^{-1} and the maximum event rainfall erosivity is 58,874 MJ·mm·ha^{-1}·h^{-1}. The storm is initially concentrated in the southeast of Henan and Anhui provinces, and the rainfall and rainfall intensity reached the peak on 20 July. At the same time, the rainstorm center moved to the north of Henan province with Zhengzhou as the center of the rainstorm. The EN of Zhengzhou Meteorological Station reached 144.2 MJ·ha^{-1} on 20 July. It can be seen that the "7.20" storm has the characteristics of long duration, heavy cumulative rainfall, a wide range of heavy rainfall, and extremely strong short-term rainfall. It is a particularly serious natural disaster that caused serious urban waterlogging, mountain floods, landslides and other disasters, resulting in heavy casualties and serious economic losses.

3.2 How extreme is the event recorded at Zhengzhou meteorological station?

3.2.1 Frequency of occurrence the maximum daily and event rainfall erosivity

Annual maximum daily rainfall erosivity and the annual maximum event rainfall erosivity in Zhengzhou meteorological station from 1951 to 2020 are shown in Fig. 6 along with fitted GEVLP-III distribution. It can be seen from Fig. 6 & 7 that the LP-III GEV distribution fits the maximum daily rainfall erosivity and the maximum event rainfall erosivity well. Using the fitted LP-IIIGEV distribution, the average recurrence interval of the maximum daily rainfall erosivity of the "7.20" rainstorm is estimated to be about 1 in 109,07923,100 years, and the ratio of the observed daily erosivity (43,354 MJ·mm·ha^{-1}·h^{-1}) over 1-in-100-year daily erosivity (4798 7551 MJ·mm·ha^{-1}·h^{-1}) is 9.045.74. Similarly, the average recurrence interval of the maximum event rainfall erosivity is estimated to be about 1 in 154,15410,000 years, the observed event erosivity of the "7.20" rainstorm (58,874 MJ·mm·ha^{-1}·h^{-1}) is 9.456.17 times larger than the 1-in-100-year event erosivity (6229544 9 MJ·mm·ha^{-1}·h^{-1}). Based on the 95% confidence interval for the LP-III distribution, the estimated return period of the maximum daily and event rainfall erosivity is most likely to be at least 785 and 516 years. Evidently, compared with observations in the past decades (1951-2020), the maximum daily and event rainfall erosivity of the "7.20" rainstorm in 2021 is extraordinary, and the event is so rare and extreme that it should be regarded as an outlier among observations in other years.

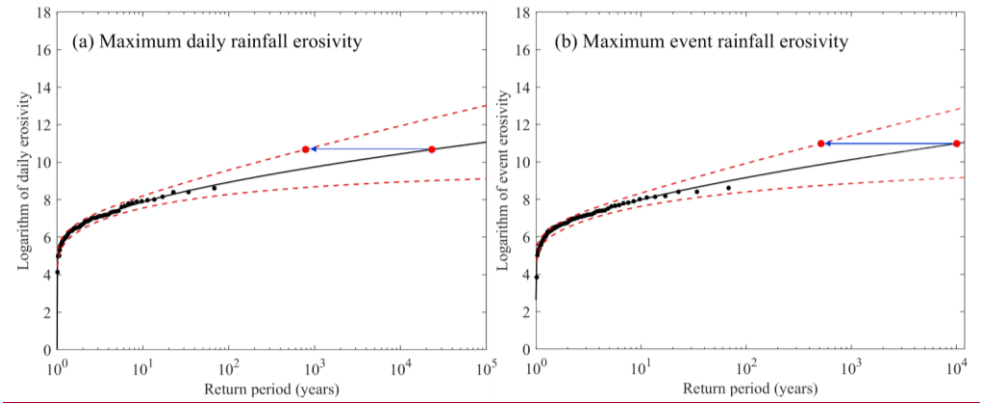

Figure 6. The logarithm of ~~Observed~~ observed daily (a) and event (b) rainfall erosivity as a function of the empirically ~~and~~ fitted return period at Zhengzhou meteorological station. Black solid circles are observations from the period 1951-2020, the red solid circles indicate the "7.20" storm in 2021, the red dotted line is the upper and lower limit of 95% confidence interval, and the solid lines in black represent the fitted P-Ⅲ distribution using the logarithm of observations from 1951-2020. ~~(black solid circles are observations from the period 1951-2020, the red solid circles indicate the "7.20" rainstorm in 2021, and the solid lines in black represent the fitted GEV distribution using observations from 1951-2020)~~

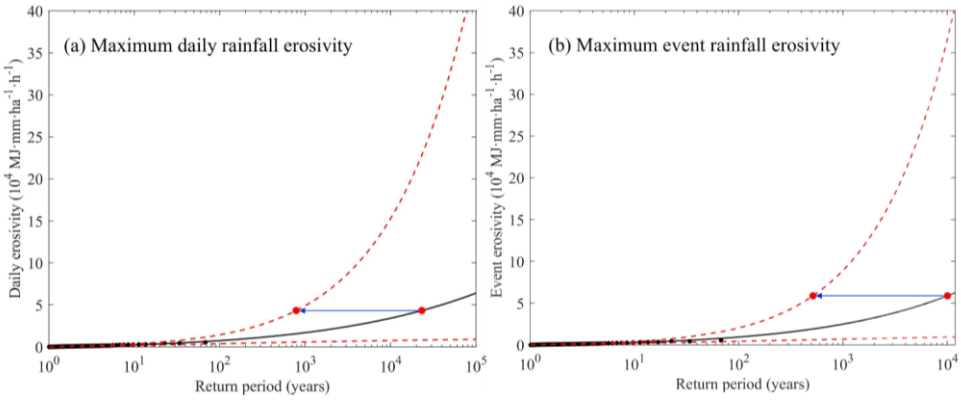

Figure 7. Observed daily (a) and event (b) rainfall erosivity as a function of the empirically fitted return period for Zhengzhou meteorological station (Perform anti-logarithm conversion for Fig. 6)

The map of the return period of maximum daily and event rainfall erosivity of the "7.20" storm in Henan province is shown in Fig. 8. Similar to Zhengzhou meteorological station, by fitting the LP-III distribution, the map of the return period of rainfall erosivity of "7.20" storm in the study area was drawn by fitting the LP-III distribution. The map shows that the return periods of daily (11 stations) and rainfall (16 stations) erosivity at some meteorological stations exceed 1-in-100-year, mainly in the northern region of Henan province, with Zhengzhou meteorological station as the center of the "7.20" storm.

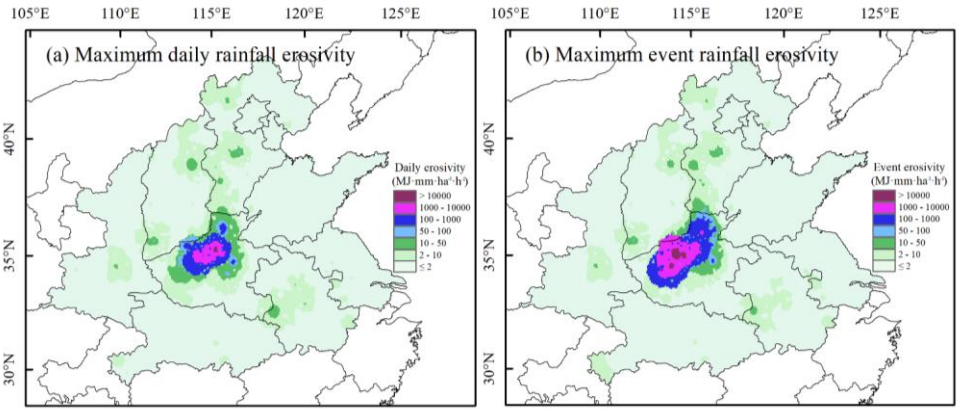

Figure 8. The return period of daily (a) and event (b) rainfall erosivity of the "7.20" storm in the study area.

3.2.2 Distribution of the maximum rainfall erosivity in different latitudes

Geographical distribution of the maximum daily rainfall erosivity ever recorded at each of 2420 meteorological stations in China is shown as a function of the latitude in Fig. ~~7~~9. Envelope curves I and II are drawn for the scatter plot, and the stations and the corresponding daily rainfall and rainfall erosivity values that were used to define these envelope curves are given in

Table. 2. The two envelope curves overlap at three stations at low latitude and one at high latitude, and the change from curve I to II in the middle latitude is entirely a result of the "7.20" ~~rain~~storm in 2021. ~~Prior to~~ Prior to the "7.20" ~~rain~~storm, curve I shows that the maximum recorded daily rainfall erosivity decreases from about 20°N as the latitude increases, and the maximum daily erosivity value was 39,345 MJ·mm·ha^{-1}·h^{-1}, recorded Maoming meteorological station in Guangdong ~~P~~province (21.75°N) on 5 June 2020. ~~Post~~ Because of the "7.20" rainstorm, the maximum daily rainfall erosivity ever recorded was increased to 43,354 MJ·mm·ha^{-1}·h^{-1} or by more than 10 % at Zhengzhou meteorological station (34.72°N) on 20 July 2021.

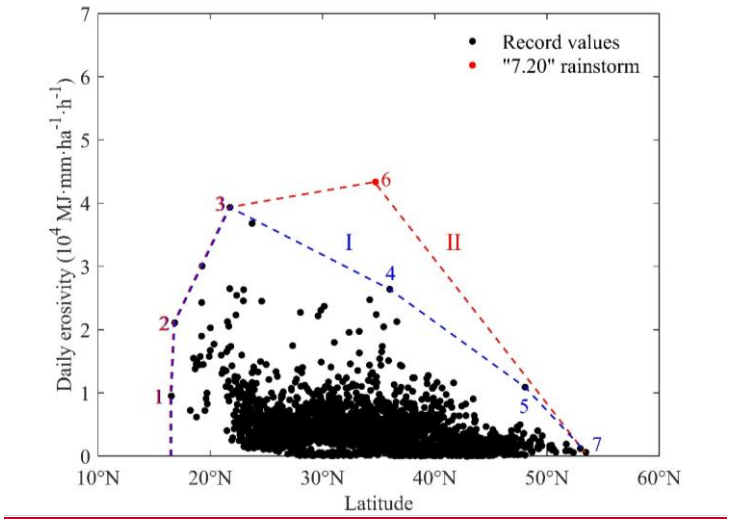

Figure ~~7~~9. The maximum recorded daily rainfall erosivity as a function of latitude for China. The point enclosed by the envelope curve I is the maximum daily rainfall erosivity of each station from 1951 to 2020. The point enclosed by envelope curve II is the maximum daily rainfall erosivity of each station from 1951 to 2021.

Table 2. The mean annual rainfall, maximum daily rainfall and rainfall erosivity for stations to define envelope curves.

ID		Station ID	Station name	Latitude	Mean annual rainfall (mm)	Daily rainfall (mm)	Daily rainfall erosivity (MJ·mm·ha^{-1}·h^{-1})	Date
I	II							
1	1	59985	Shanhu	16.53	1316.0	227.6	9512	1980-09-12
2	2	59981	Xisha	16.83	1467.9	585.6	21104	1995-09-05
3	3	59659	Maoming	21.75	1701.7	307.3	39345	2020-06-05
4		54848	Zhucheng	35.98	623.8	592	26398	1999-08-12
5		50658	Keshan	48.05	445.4	179.6	10909	1957-07-15
	6	57083	Zhengzhou	34.72	566.7	552.5	43354	2021-07-20
7	7	50137	Beijicun	53.47	385.2	77.6	603	2010-07-31

Geographical distribution of the maximum event rainfall erosivity ever recorded at each of 2420 meteorological stations in China is shown as a function of the latitude in Fig. ~~8~~10. Envelope curves I and II are drawn for the scatter plot, and the stations and the corresponding event rainfall and rainfall erosivity values that were used to define these envelope curves are given in Table. 3. The two envelope curves overlap at three stations at low latitude and one at high latitude, and the change from curve I to II in the middle latitude is entirely a result of the extreme "7.20" ~~rain~~storm in 2021. ~~Prior to~~ Prior to the "7.20" ~~rain~~storm, curve I shows that the maximum recorded event rainfall erosivity decreases from about 20°N as the latitude increases, and the maximum ever event erosivity value was 41,537 MJ·mm·ha^{-1}·h^{-1}, recorded Maoming meteorological station in Guangdong ~~Province~~ province (21.75°N) from 20:00 on 20 May 1987 to 18:00 on 22 May 1987. ~~Post~~Because of the "7.20" ~~rain~~storm, the

maximum event rainfall erosivity ever recorded was increased to 58,874 MJ·mm·ha^{-1}·h^{-1}, or an increase of more than 40 % at Zhengzhou meteorological station (34.72°N) on 20 July 2021.

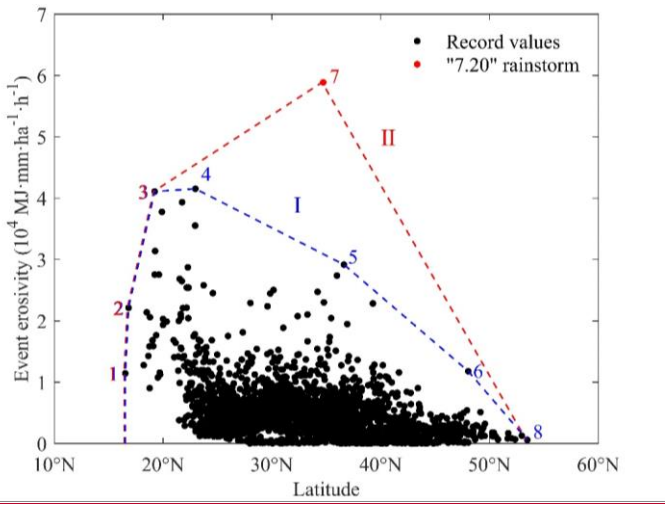

Figure ~~8~~10. The maximum recorded event rainfall erosivity as a function of latitude for China. The point enclosed by the envelope curve I is the maximum event rainfall erosivity of each station from 1951 to 2020. The point enclosed by envelope curve II is the maximum event rainfall erosivity of each station from 1951 to 2021.

Table 3. The mean annual rainfall, maximum event rainfall and rainfall erosivity for stations to define envelope curves.

ID		Station ID	Station name	Latitude	Starting date and time	End date and time	Mean annual rainfall (mm)	Event rainfall (mm)	Event rainfall erosivity (MJ·mm·ha^{-1}·h^{-1})
I	II								
1	1	59985	Shanhu	16.53	1980-09-11 11:00	1980-09-12 8:00	1316.0	288.2	11446
2	2	59981	Xisha	16.83	1995-09-05 8:00	1995-09-06 23:00	1467.9	625.5	22135
3	3	59855	Qionghai	19.23	2010-10-01 22:00	2010-10-08 15:00	2021.7	1433.3	41083
4		59500	Haifeng	22.97	1987-05-20 20:00	1987-05-22 18:00	2407.5	987.3	41537
5		53892	Handan	36.62	1963-08-03 3:00	1963-08-06 1:00	478.8	748.1	29174
6		50658	Keshan	48.05	1957-07-15 14:00	1957-07-15 24:00	445.4	199.5	11794
	7	57083	Zheng-zhou	34.72	2021-07-18 8:00	2021-07-21 10:00	566.7	785.1	58874
8	8	50137	Beijicun	53.47	2010-07-30 23:00	2010-07-31 14:00	385.2	77.6	603

A large number of studies have shown that the mean annual rainfall and rainfall erosivity, i.e. the R-factor, decrease from southeast to northwest in China (Yin et al., 2019; Yue et al., 2022), that is, the mean annual rainfall and rainfall erosivity is~~are~~ the highest at low latitude in China. Like rainfall, the average rainfall intensity for given storm duration also tends to be high at low latitude, and low at high latitude in China (Kong et al., 2017 ~~(Bureau of Hydrology et al., 2001)~~). Thus, one would expect that maximum daily and event rainfall erosivity tends to decrease with the latitude, a trend largely supported by the envelope curve I in Fig. ~~7~~9 & ~~8~~10. The "7.20" ~~rain~~storm may have fundamentally changed the nature and distribution of extreme daily and event erosivity in China as we knew them up to now. This is consistent with the research of Wang ~~et al.~~and Luo (~~2002~~2006), and the ~~rain~~storm extreme value does not always conform to the pattern of decreasing from low latitude to high latitude. For

example, based on measured and surveyed rainfall records, the maximum 24-hour rainfall depth occurred at Linzhuang ~~meteorological Station~~ in Henan p~~P~~rovince in the mid-latitude on 5~~–~~7 August 1975 (Ding., 2015~~Wang et al., 2002~~). Occurrence of this "7.20" ~~rain~~storm ~~event~~ in 2021 around Zhengzhou has important implications. First, Figure. ~~7~~ 9 & ~~8~~ 10 suggest that extreme event erosivity may be the highest in mid-latitude around 35°N despite the fact the mean annual rainfall and rainfall intensity are by no means the highest in mid-latitude in China. Second, the "7.20" ~~rain~~storm was so rare and freakish that the event was seemingly unrelated to the underlying climatology. Finally, the "7.20" ~~rain~~storm has led us to realize that such extreme erosive events could and may occur anywhere in eastern China with further implications for soil conservation planning.

4 Conclusions

This study assessed an~~evaluated the~~ extreme rainfall event~~s~~ in Henan ~~P~~province from 20:00 on 16 July 2021 to 20:00 on 22 July 2021, using hourly rainfall data from 796 stations in Henan and surrounding provinces. Based on hourly rainfall data of 2420 meteorological stations in China from 1951 to 2021, the annual maximum daily ~~rainfall erosivity and the annual maximum~~ and event rainfall erosivity of Zhengzhou meteorological ~~S~~station ~~are~~ were fitted with the ~~GEV~~LP-III distribution to ~~assess the~~evaluate magnitude and frequency of occurrence of this extreme event in terms of rainfall amount and erosivity values.~~.~~ The following conclusions can be drawn as follows:

(1) The maximum event rainfall (785.1 mm), maximum daily rainfall (552.5 mm), maximum hourly rainfall intensity (201.9 $mm \cdot h^{-1}$) and maximum event rainfall erosivity (58,874 $MJ \cdot mm \cdot ha^{-1} \cdot h^{-1}$) of "7·20" ~~rain~~storm all occurred and were recorded at Zhengzhou meteorological station. The period of the highest rainfall intensity was mainly concentrated in the middle and late stages of the storm, reaching its peak on 20 July, producing a daily total of 144.2 $MJ \cdot ha^{-1}$ energy.

(2) Based on long-term observations ~~in the past decades (~~for the period 1951-2020~~)~~ and the fitted LP-III~~GEV~~ distribution, the "7.20" ~~rain~~storm was estimated to have an average recurrence interval in excess of 10,0~~,0~~0~~0~~0 years, and the annual maximum daily and event rainfall erosivity were about ~~10~~ six times larger than 1-in-100-year erosivity values.

(3) This extreme event recorded at the Zhengzhou meteorological station has set a new record for daily and event rainfall erosivity values in mainland China. The "7.20" rainstorm in 2021 was so rare and freakish, and suggested to us that extreme erosive events could and may occur anywhere in eastern China, rather than in low latitude with high rainfall amount and rainfall intensity as we previously knew and expected.

Author contributions. ~~Not applicable.~~Observed hourly rainfall data from National Meteorological Information Center of the China Meteorological Administration (NMIC, http://data.cma.cn).

Author contributions. Y Xiao, S Yin and B Yu conceived and designed this study.~~developed the concepts of the manuscript.~~ Y Xiao undertook data analysis and interpretation, prepared all the diagrams, and drafted the manuscript.~~conducted calculations and visualization, and wrote the first draft.~~ S Yin and B Yu guided data analysis and interpretation.~~did methodology, review and editing.~~ All authors reviewed and edited the manuscript.~~C Fan, W Wang and Y Xie did the review and editing.~~

Competing interests. The authors declare that they have no conflict of interest.

Disclaimer. Publisher's note: Copernicus Publications remains neutral with regard to jurisdictional claims in published maps and institutional affiliations.

Financial support. This research has been supported by the National Key Research and Development Program of China (grant

no. 2021YFE0113800), National Natural Science Foundation of China (grant no. 41877068) and the project “ACRP 13: Soil erosion in Austria -from mean to extreme (EROS-A)” funded by the Klima- und Energiefonds.

References

Alexander, L.V., Hope, P., Collins, D., Trewin, B., Lynch, A., and Nicholls, N.: Trends in Australia's climate means and extremes: a global context, Aust. Met~~eorol~~. Mag., 56, 1–18, 2007.

Almagro, A., Oliveira, T. P. S., Nearing, M. A., and Hagemann, S.: Projected climate change impacts in rainfall erosivity over Brazil, Sci. Rep., 7, 8130, https://doi.org/10.1038/s41598-017-08298-y, 2017.

Bobeé, B. B., and Robitaille, R.: The Use of the Pearson Type 3 and Log Pearson Type 3 Distributions Revisited, Water Resour. Res., 13(2), 427–443, https://doi.org/10.1029/WR013i002p00427, 1977.~~Auerswald, K., Fischer, F. K., Winterrath, T., and Brandhuber, R.: Rain erosivity map for Germany derived from contiguous radar rain data, Hydrol. Earth Syst. Sci., 23, 1819–1832, https://doi.org/10.5194/hess-23-1819-2019, 2019.~~

~~Bureau of Hydrology, Changjiang Water Resources Commission, and Nanjing Institute of Hydrology and Water Resources.: Handbook of calculation design flood for water resources and hydropower projects, Hydropower and Electrical Press, Beijing, 2001. (in Chinese)~~

Borrelli, P., Diodato, N., and Panagos, P.: Rainfall erosivity in Italy: a national scale spatio-temporal assessment, Int. J. Digit. Earth., 9(9), 835–850. https://doi.org/10.1080/17538947.2016.1148203, 2016.

Bezak, N., Mikoš, M., Borrelli, P., Liakos, L., and Panagos, P.: An in-depth statistical analysis of the rainstorms erosivity in Europe, Catena, 206, 105577, https://doi.org/10.1016/j.catena.2021.105577, 2021.

Bezak, N., Borrelli, P., and Panagos, P.: Exploring the possible role of satellite-based rainfall data in estimating inter- and intra-annual global rainfall, Hydrol. Earth Syst. Sci., 26, 1907-1924, https://doi.org/10.5194/hess-26-1907-2022, 2022

~~Cao, Y., Wang, S. J., Bai, X. Y., Li, H. W., Wang, M. M., and Wu, L. H.: Inversion calculation and spatial-temporal pattern of rainfall erosivity in southwestern China over one hundred years, Acta Ecol. Sin., 38, 8766–8773, https://doi.org/10.5846/stxb201805241142, 2018. (in Chinese)~~

Diodato, N., Bellocchi, G., Romano, N., and Guadagno, F. M.: Modelling the rainfall erosivity of the Rhone Region (Southeastern France) associated with climate variability and storminess, Adv. Meteorol., 2016, 7626505, https://doi.org/10.1155/2016/7626505, 2016.

Ding, Y. H.: On the study of the unprecedented heavy rainfall in Henan Province during 4-8 August 1975: Review and assessment, Acta Meteorol. Sin. (in Chinese), 73(3): 411–424, http://dx.chinadoi.cn/10.11676/qxxb2015.067, 2015.

England, J. F., Jr., Salas, J. D. and Jarrett, R. D.: Comparisons of two moments-based estimators that utilize historical and paleoflood data for the log Pearson type III distribution, Water Resour. Res., 39(9), 1243, https://doi.org/10.1029/2002WR001791, 2003.

England, J. F., Jr., Cohn, T. A., Faber, B. A., Stedinger, J. R., Thomas, W. O., Jr., Veilleux, A. G., Kiang, J. E., and Mason, R.: Guidelines for Determining Flood Flow Frequency-Bulletin 17C, Techniques and Methods 4-B5, U.S. Geological Survey, Reston, VA, USA, 2019.

Evans, J.P., Arguesco, D., Olson, R., and Di Luca, A.: Bias-corrected regional climate projections of extreme rainfall in south-east Australia, Theor. Appl. Climatol., 130(3–4), 1085–1098, https://doi.org/10.1007/s00704-016-1949-9, 2016.

~~Fishman, R.: More uneven distributions overturn benefits of higher precipitation for crop yields, Environ. Res. Lett., 11, 024004, https://doi.org/10.1088/1748-9326/11/2/024004, 2016.~~

Fang, W., Huang, Q., Huang, S. Z., Yang, J., Meng, E. H., and Li, Y. Y.: Optimal sizing of utility-scale photovoltaic power

generation complementarily operating with hydropower: a case study of the World's largest hydro-photovoltaic plant, Energy Convers. Manag., 136, 161–172, https://doi.org/10.1016/j.enconman.2017.01.012, 2017.

Fang, W., Huang, S.Z., Huang, Q., Huang, G. H., Meng, E. H., and Luan, J. K.: Reference evapotranspiration forecasting based on local meteorological and global climate information screened by partial mutual information, J. Hydrol., 561, 764–779, https://doi.org/10.1016/j.jhydrol.2018.04.038, 2018.

Fishman, R.: More uneven distributions overturn benefits of higher precipitation for crop yields, Environ. Res. Lett., 11(2), 024004, https://doi.org/10.1088/1748-9326/11/2/024004, 2016.

Gu, Z. J., Feng, D. T., Duan, X. W., Gong, K. F., Li, Y. W., and Yue, T. Y.: Spatial and Temporal Patterns of Rainfall Erosivity in the Tibetan Plateau, Water, 12(1), 200, https://doi.org/10.3390/w12010200, 2020.

~~Hosking, J. R. M.: L-Moments: Analysis and Estimation of Distributions Using Linear Combinations of Order Statistics, J. R. Stat. Soc., Ser. B., Methodol., 52, 105–124, http://www.jstor.org/stable/2345653, 1990.~~

Huang, S. Z., Chang, J. X., Huang, Q., Chen, Y. T., and Leng, G.Y.: Quantifying the relative contribution of climate and human impacts on runoff change based on the Budyko hypothesis and SVM model, Water Resour. Manag., 30(7), 2377–2390, https://doi.org/10.1007/s11269-016-1286-x, 2016a.

Huang, S., Huang, Q., Chang, J.X., and Leng, G. Y.: Linkages between hydrological drought, climate indices and human activities: a case study in the Columbia River basin, Int. J. Climatol., 36(1), 280–290, https://doi.org/10.1002/joc.4344, 2016b.

Huang, S., Huang, Q., Leng, G.Y., and Chang, J. X.: A hybrid index for characterizing drought based on a nonparametric kernel estimator, J. Appl. Meteorol. Climatol., 55(6), 1377–1389, https://doi.org/10.1175/JAMC-D-15-0295.1, 2016c.

~~Huang, Y. X., Liang, Z. M., Hu, Y. M., Li, B. Q., and Wang, J.: Theoretical derivation for the exceedance probability of corresponding flood volume of the equivalent frequency regional composition method in hydrology, Hydrol. Res., 51, 1274–1292, https://doi.org/10.2166/nh.2020.027, 2020.~~

IPCC.: Climate Change 2021: The Physical Science Basis, Working Group I contribution to the Sixth Assessment Report of the Intergovernmental Panel on Climate Change, Masson-Delmotte, V., Zhai, P., Pirani, A., Connors, S. L., Péan, C., Berger, S., Caud, N., Chen, Y., Goldfarb, L., Gomis, M. I., Huang, M., Leitzell, K., Lonnoy, E., Matthews, J. B. R., Maycock, T. K., Waterfield, T., Yelekçi, O., Yu, R., and Zhou, B. (Eds.)~~P. Zhai, A. Pirani, S.L. Connors, C. Péan, S. Berger, N. Caud, Y. Chen, L. Goldfarb, M.I. Gomis, M. Huang, K. Leitzell, E. Lonnoy, J.B.R. Matthews, T.K. Maycock, T. Waterfield, O. Yelekçi, R. Yu, and B. Zhou (eds.)~~. Cambridge University Press, Cambridge, United Kingdom and New York, NY, USA, In press, https://doi.org/10.1017/9781009157896, 2021.

Jiang, Q., Li, W., Wen, J., Fan, Z., Chen, Y., Scaioni, M., and Wang, J.: Evaluation of satellite-based products for extreme rainfall estimations in the eastern coastal areas of China, J. Integr. Environ. Sci., 16(1), 191–207, https://doi.org/10.1080/1943815X.2019.1707233, 2019.

Jin, S. Y., Guo, S. M., and H, W. B.: Analysis on the Return Period of "7.20" Rainstorm in the Xiaohua Section of the Yellow River in 2021, Water, 14(15), 2444, https://doi.org/10.3390/w14152444, 2022.

Kebede, S. Y., Endalamaw, T. N., Sinshaw, G. B., and Atinkut, B. H.: Modeling soil erosion using RUSLE and GIS at watershed level in the upper beles, Ethiopia, Environ. Challenges, 2, 100009, https://doi.org/10.1016/j.envc.2020.100009, 2021.

~~Klik, A., and Rosner, J.: Long-term experience with conservation tillage practices in Austria: Impacts on soil erosion processes, Soil Tillage Res., 203, 104669, https://doi.org/10.1016/j.still.2020.104669, 2020.~~

Kilic, O. M. and Gunal, H.: Spatial-temporal changes in rainfall erosivity in Turkey using CMIP5 global climate change scenario, Arabian J. Geosci., 14, 1079, https://doi.org/10.1007/s12517-021-07184-2, 2021.

Kinnel, P. I. A.: Rainfall intensity-kinetic energy relationships for soil loss prediction, Soil Sci. Soc. Am. J., 45(1), 153–155,

带格式的: 字体: (中文) +中文正文 (等线)

带格式的: 缩进: 左侧: 0 厘米, 首行缩进: 0 字符

https://doi.org/10.2136/sssaj1981.03615995004500010033x, 1981.

Kite, G. W.: Confidence limits for design events, Water Resour. Res., 11(1): 48–53, https://doi.org/10.1029/WR011i001p00048, 1975.

Klik, A., and Rosner, J.: Long-term experience with conservation tillage practices in Austria: Impacts on soil erosion processes, Soil Tillage Res., 203, 104669, https://doi.org/10.1016/j.still.2020.104669, 2020.

Kong, F., Lu, L. L., and Fang, J.: Spatiotemporal pattern of hourly heavy rainfall in China and its spatial correlation with urbanization factors during 1991–2010, Climatic and Environmental Research (in Chinese), 22(3): 355–364, 10.3878/j.issn.1006–9585.2017.16139, 2017.

~~Klik, A., Haas, K., Dvoracekova, A., and Fuller, I. C.: Spatial and temporal distribution of rainfall erosivity in New Zealand, Soil Res., 53, 815–825, https://doi.org/10.1071/SR14363, 2015.~~

~~Kebede, S. Y., Endalamaw, T. N., Sinshaw, G. B., and Atinkut, B. H.: Modeling soil erosion using RUSLE and GIS at watershed level in the upper beles, Ethiopia, Environ. Challenges, 2, 100009, https://doi.org/10.1016/j.envc.2020.100009, 2021.~~

~~Lu, H. and Yu, B.: Spatial and seasonal distribution of rainfall erosivity in Australia, Soil Res., 40, 887–901, https://doi.org/10.1071/SR01117, 2002.~~

Liu, B. Y., Zhang, K. L., and Xie, Y.: An empirical soil loss equation. Proceedings-Process of Soil Erosion and Its Environment Effect, 2, 21–25, 2002.

Li, J., Liu, Z. H., and Li, R.: Temporal and spatial characteristics of rainfall erosivity with different geomorphology types on the loess plateau, Bull. Soil Water Conserv. (in Chinese), 28(3), 124–127, https://doi.org/10.13961/j.cnki.stbctb.2008.03.025, 2008. ~~(in Chinese)~~

Liu, S. Y., Huang, S. Z., Huang, Q., Xie, Y. Y., Leng, G. Y., Luan, J. K., Song, X. Y., Wei, X., and Li, X. Y.: Identification of the non-stationarity of extreme precipitation events and correlations with large-scale ocean-atmospheric circulation patterns: A case study in the Wei River Basin, China, J. Hydrol., 548, 184–195, https://doi.org/10.1016/j.jhydrol.2017.03.012, 2017.~~Li, J., Yu, R. C., and Sun, W.: Duration and Seasonality of Hourly Extreme Rainfall in the Central Eastern China, Acta Meteorol. Sin., 27, 799–807, https://doi.org/10.1007/s13351-013-0604-y, 2013.~~

Liu, S. L., Huang, S. Z., Xie, Y. Y., Leng, G. Y., Huang, Q., Wang, L., and Xue, Q.: Spatial-temporal changes of rainfall erosivity in the loess plateau, China: Changing patterns, causes and implications, Catena, 166, 279–289, https://doi.org/10.1016/j.catena.2018.04.015, 2018.

Liao, X., Xu, W., Zhang, J., Li, Y., and Tian, Y.: Global exposure to rainstorms and the contribution rates of climate change and population change, Sci. Total Environ., 663, 644–653, https://doi.org/10.1016/j.scitotenv.2019.01.290, 2019.

McGregor, K. C., Bingner, R. L., Bowie, A. J., and Foster, G. R.: Erosivity index values for northern Mississippi, Trans. ASAE, 38(4), 1039–1047, https://doi.org/10.13031/2013.27921, 1995.

~~Michaelsen, J.: Cross-validation in statistical climate forecast models, J. Appl. Meteor., 26, 1589–1600, https://doi.org/10.1175/1520-0450(1987)026<1589:CVISCF>2.0.CO;2, 1987.~~

Meusburger, K., Steel, A., Panagos, P., Montanarella, L., and Alewell, C.: Spatial and temporal variability of rainfall erosivity factor for Switzerland, Hydrol. Earth Syst. Sci., 16, 167–177, https://doi.org/10.5194/hess-16-167-2012, 2012.

~~Mello, C. R., Viola, M. R., Beskow, S., and Norton, L. D.: Multivariate models for annual rainfall erosivity in Brazil, Geoderma, 202, 88–102, https://doi.org/10.1016/j.geoderma.2013.03.009, 2013.~~

~~Ma, X., He, Y., Xu, J., van Noordwijk, M., and Lu, X.: Spatial and temporal variation in rainfall erosivity in a Himalayan watershed, Catena, 121, 248–259, https://doi.org/10.1016/j.catena.2014.05.017, 2014.~~

带格式的: 字体: (中文) +中文正文 (等线)

带格式的: 字体: (中文) +中文正文 (等线)

McGehee, R. P., Flanagan, D. C., Srivastava, P., Engel, B. A., Huang, C. H., and Nearing, M. A.: An updated isoerodent map of the conterminous United States, ISWCR, 10, 1–16, https://doi.org/10.1016/j.iswcr.2021.06.004, 2022.

Nearing, M. A., Pruski, F. F., and O'Neal, M. R.: Expected climate change impacts on hillslope erosion rates: a review, J. Soil Water Conserv., 59, 43–50, 2004.

Palharini, R. S. A., Vila, D. A., Rodrigues, D. T., Quispe, D. P., Palharini, R. C., de Siqueira, R. A., and de Sousa Afonso, J. M.: Assessment of the extreme precipitation by satellite estimates over South America, Remote Sens., 12(13), 2085, https://doi.org/10.3390/rs12132085, 2020.

Petek, M., Mikoš, M., and Bezak, N.: Rainfall erosivity in Slovenia: Sensitivity estimation and trend detection, Environ. Res., 167, 528–535, https://doi.org/10.1016/j.envres.2018.08.020, 2018.

Panagos, P., Ballabio, C., Borrelli, P., Meusburger, K., Klik, A., Rousseva, S., Tadic, M. P., Michaelides, S., Hrabalikova, M., Olsen, P., Aalto, J., Lakatos, M., Rymszewicz, A., Dumitrescu, A., Begueria, S., and Alewell, C.: Rainfall erosivity in Europe, Sci. Total Environ., 511, 801–814, https://doi.org/10.1016/j.scitotenv.2015.01.008, 2015.

Panagos, P., Borrelli, P., Spinoni, J., Ballabio, C., Meusburger, K., Begueria, S., Klik, A., Michaelides, S., Petan, S., Hrabalikova, M., Olsen, P., Aalto, J., Lakatos, M., Rymszewicz, A., Dumitrescu, A., Tadic, M. P., Diodato, N., Kostalova, J., Rousseva, S., Banasik, K., and Alewell, C.: Monthly rainfall erosivity: Conversion factors for different time resolutions and regional assessments, Water, 8, 119, https://doi.org/10.3390/w8040119, 2016.

Panagos, P., Borrelli, P., Meusburger, K., Yu, B. F., Klik, A., Lim, K. J., Yang, J. E., Ni, J. R., Miao, C. Y., Chattopadhyay, N., Sadeghi, S. H., Hazbavi, Z., Zabihi, M., Larionov, G. A., Krasnov, S. F., Gorobets, A. V., Levi, Y., Erpul, G., Birkel, C., Hoyos, N., Naipal, V., Oliveira, P. T. S., Bonilla, C. A., Meddi, M., Nel, W., Al Dashti, H., Boni, M., Diodato, N., Van Oost, K., Nearing, M., and Ballabio, C.: Global rainfall erosivity assessment based on high-temporal resolution rainfall records. Sci. Rep., 7, 4175, https://doi.org/10.1038/s41598-017-04282-8, 2017.

Petek, M., Mikoš, M., and Bezak, N.: Rainfall erosivity in Slovenia: Sensitivity estimation and trend detection, Environ. Res., 167, 528–535, https://doi.org/10.1016/j.envres.2018.08.020, 2018.

Panagos, P., Borrelli, P., Matthews, F., Liakos, L., Bezak, N., Diodato, N., and Ballabio, C.: Global rainfall erosivity projections for 2050 and 2070, J. Hydrol., 610, 127865, https://doi.org/10.1016/j.jhydrol.2022.127865, 2022.

Qin, W., Guo, Q., Zuo, C., Shan, Z., Ma, L., and Sun, G.: Spatial distribution and temporal trends of rainfall erosivity in mainland China for 1951–2010, Catena, 147, 177–186, https://doi.org/10.1016/j.catena.2016.07.006, 2016.Qian, H. W., Kong, H. J., Zhao, P. J., Ren, J. J., and Zhang, Y. Y.: Anomaly-based versus full-field-based weather analysis on the extraordinary storm in Henan province in July 2021. Chinese J. Geophys. (in Chinese), 65(11): 4208–4224, https://doi.org/10.6038/cj92022P0631, 2022.

Rahmawati, N., and Lubczynski, M. W.: Validation of satellite daily rainfall estimates in complex terrain of Bali Island, Indonesia, Theor. Appl. Climatol., 134, 513–532, https://doi.org/10.1007/s00704-017-2290-7, 2018

Renard, K. G., Foster, G. R., Weesies, G. A., McCool, D. K., and Yoder, D. C.: Predicting soil erosion by water: a guide to conservation planning with the revised universal soil loss equation (RUSLE), Agriculture Handbook, US Department of Agriculture, Washington, D. C., 1997.

Sadeghi, S. H. R., Zabihi, M., Vafakhah, M., and Hazbavi, Z.: Spatiotemporal mapping of rainfall erosivity index for different return periods in Iran, Nat. Hazards, 87, 35–56, https://doi.org/10.1007/s11069-017-2752-3, 2017.

USDA-ARS.: Science documentation: Revised universal soil loss equation version2 (RUSLE2), US Department of Agriculture, Agricultural Research Service, Washington, D.C., 2013.

Viessman Jr., W. and Lewis, G.: Introduction to hydrology. Pearson Education Inc, San Antonio, U.S.A, 2002.

Wang, J. Q., and Luo, C. C.: Research on the characteristics of rainstorms and floods in China, Journal of China Hydrology

带格式的: 字体: (中文) +中文正文 (等线)

带格式的: 缩进: 左侧: 0 厘米, 首行缩进: 0 字符

(in Chinese), 26(3), 33-36, https://doi.org/10.3969/j.issn.1000-0852.2006.03.009, 2006.Wang, J. Q.: Rainstorm in China, China Water & Power Press, Beijing, 2002. (in Chinese)

Wang, W. T., Yin, S. Q., Xie, Y., Liu, B. Y., and Liu, Y. N.: Effects of four storm patterns on soil loss from five soils under natural rainfall, Catena, 141, 56–65, https://doi.org/10.1016/j.catena.2016.02.019, 2016.

Wang, W., Yin, S. Q., Gao, G., Papalexiou, S. M., and Wang, Z.: Increasing trends in rainfall erosivity in the Yellow River basin from 1971 to 2020, J. Hydrol., 610, 127851, https://doi.org/10.1016/j.jhydrol.2022.127851, 2022.

Wischmeier, W. H. and Smith, D. D.: Rainfall energy and its relationship to soil loss, Trans. Am. Geophys. Union, 39, 285–291, https://doi.org/10.1029/TR039i002p00285, 1958.

Wischmeier, W. H. and Smith, D. D.: Predicting rainfall erosion losses from cropland east of the Rocky Mountains, Agriculture Handbook, US Department of Agriculture, Washington, D. C., 1965.

Wischmeier, W. H. and Smith, D. D.: Predicting rainfall erosion losses: A guide to conservation planning, Agriculture Handbook, US Department of Agriculture, Washington, D. C., 1978.

Wang, W. T., Yin, S. Q., Xie, Y., Liu, B. Y., and Liu, Y. N.: Effects of four storm patterns on soil loss from five soils under natural rainfall, Catena, 141, 56–65, https://doi.org/10.1016/j.catena.2016.02.019, 2016.

Wang, W., Yin, S. Q., Gao, G., Papalexiou, S. M., and Wang, Z.: Increasing trends in rainfall erosivity in the Yellow River basin from 1971 to 2020, J. Hydrol., 610, 127851, https://doi.org/10.1016/j.jhydrol.2022.127851, 2022.

Xie, Y., Liu, B. Y., and Zhang, W. B.: Study on standard of erosive rainfall, J. Soil Water Conserv., 14, 6-11, https://doi.org/10.13870/j.cnki.stbcxb.2000.04.002, 2000. (in Chinese)

Xie, Y., Yin, S. Q., Liu, B., Nearing, M. A., and Zhao, Y.: Models for estimating daily rainfall erosivity in China, J. Hydrol., 535, 547–558, https://doi.org/10.1016/j.jhydrol.2016.02.020, 2016.

Yang, F. and Lu, C.: Spatiotemporal variation and trends in rainfall erosivity in China's dryland region during 1961–2012, Catena, 133, 362–372, https://doi.org/10.1016/j.catena.2015.06.005, 2015.

Yin, S. Q. and Wang, W. T.: A review on the stochastic simulation of rainfall process data for soil erosion assessment, Prog. Geogr., 39, 1747–1757, https://doi.org/1007-6301(2020)39:10<1747:TRQSYJ>2.0.TX;2-4, 2020. (in Chinese)

Yin, S., Xie, Y., Liu, B. and Nearing, M.A.: Rainfall erosivity estimation based on rainfall data collected over a range of temporal resolutions, Hydrol. Earth Syst. Sci., 12, 4965–4996, https://doi.org/10.5194/hessd-12-4965-2015, 2015.

Yin, S. Q., Nearing, M. A., Borrelli, P., and Xue, X. C.: Rainfall Erosivity: An Overview of Methodologies and Applications, Vadose Zone J., 16(12), https://doi.org/10.2136/vzj2017.06.0131, 2017.

Yin, S., Xue, X., Yue, T., Xie, Y. and Gao, G.: Spatiotemporal distribution and return period of rainfall erosivity in China, Trans. Chinese Soc. Agric. Eng. (in Chinese), 35, 105–113, https://doi.org/1002-6819(2019)35:9<105:ZGJYQS>2.0.TX;2-W, 2019. (in Chinese)

Yue, T. Y., Xie, Y., Yin, S. Q., Yu, B. F., Miao, C. Y., and Wang, W. T.: Effect of time resolution of rainfall measurements on the erosivity factor in the USLE in China, ISWCR, 8, 373-382, https://doi.org/10.1016/j.iswcr.2020.06.001, 2020.

Yue, T. Y., Yin, S. Q., Xie, Y., Yu, B. F., and Liu, B. Y.: Rainfall erosivity mapping over mainland China based on high-density hourly rainfall records, Earth Syst. Sci. Data, 14, 665–682, https://doi.org/10.5194/essd-14-665-2022, 2022.

Zhou, P. H. and Wang, Z. L.: A study on rainstorm causing soil erosion in the Loess Plateau, J Soil Water Conserv. (in Chinese), 6(3), 1–5, https://doi.org/10.13870/j.cnki.stbcxb.1992.03.001, 1992.(in Chinese)

Zhu, Z. L. and Yu, B. F.: Validation of rainfall erosivity estimators for mainland China, Trans. ASABE, 58, 61–71, https://doi.org/10.13031/trans.58.10451, 2015.

Zhang, Y., Nearing, M. A., Zhang, X. C., Xie, Y., and Wei, H.: Projected rainfall erosivity changes under climate change from

带格式的: 字体: (中文) +中文正文 (等线)

multimodel and multiscenario projections in Northeast China, J. Hydrol., 384, 97–106, https://doi.org/10.1016/j.jhydrol.2010.01.013, 2010.

Zhang, X., Yang, H., Wang, X. M., Shen, L., Wang, D., and Li, H.: Analysis on characteristic and abnormality of atmospheric circulations of the July 2021 extreme precipitation in Henan, Trans. Atmos. Sci. (in Chinese), 44(5), 672–687, https://doi.org/10.13878/j.cnki.dqkxxb.20210907001, 2021. (in Chinese)

Zhang, X. K., Feng, L. C., and Cui, X. L.: Study on urban resilient waterlogging control system under 7.20 rainstorm in Zhengzhou — Core area of Fuzhou Binhai New Town, J, Catastrophol. (in Chinese), 37(2), 79-83, https://doi.org/10.3969/j.issn.1000811X.2022.02.014, 2022. (in Chinese)